Large dynamic range wavefront sensor based on a cylindrical microlens array

M. Ares and S.Royo

Center for Sensor, Instrumentation and System Development, Technical University of Catalunya (www.cd6.upc.edu)
Rambla Sant Nebridi 10, E08222 Terrassa Spain

ABSTRACT

The trade-off between resolution and dynamic range must be managed in the design of a Shack-Hartmann wavefront sensor (SHWS). A relatively large *f*-number of the microlenses should be chosen to get good lateral and vertical resolutions, but the corresponding dynamic range of measurement is degraded. To extend the dynamic range while keeping a good resolution, we propose a novel SHWS based on a cylindrical microlens array. Instead of the conventional spot pattern, two orthogonal line patterns with the microcylinders oriented in the horizontal and vertical directions are detected on a conventional CCD array. Because the sampled data are now connected along continuous lines, a self-developed line-tracking algorithm unequivocally localizes them even if they are highly distorted. With the sensor constructed, a wavefront transmitted by a commercial progressive addition lens with more than 80λ peak-to-valley height has been succesfully measured. The vertical resolution of the sensor was also calculated, resulting of $\lambda/25$ at the wavelength used (λ=635 nm).

Keywords: Wavefront sensor, Shack-Hartmann sensor, Dynamic range expansion, Single shot wavefront measurement

1. INTRODUCTION

The Shack-Hartmann wavefront sensor (SHWS) is widely used for wavefront measurements in different applications [1-3]. In a single shot, the wavefront is spatially sampled using a microlens array which creates a spot distribution on a photodetector (typically a CCD camera) placed at the focal distance of the microlenses. The relative displacement between the spots created by the wavefront to be tested and the spots of a reference wavefront (usually a flat wavefront), allows the measurement of the average wavefront slopes across each microlens aperture. Finally, the original wavefront shape is usually reconstructed by fitting the slope data to a polynomial basis [4,5].

Although the typical resolution values of the SHWS are not as high as those obtained in interferometry, the SHWS has a much larger dynamic range and a larger tolerance to non-vibration-isolated environments, allowing, for instance, the in-situ monitoring of lenses that are fabricated through an industrial manufacturing process. The trade-off between

resolution and dynamic range must be managed in the design of the sensor by choosing the *f*-number of the lenslets which best matches the requirements of the specific application [6]. If the *f*-number of the microlenses is quite large, good lateral and vertical resolutions are achieved, although the dynamic range of measurement is degraded. The opposite situation appears when a relatively short *f*-number is chosen. To be able to measure the wavefront, each of the detected spots on the CCD must be assigned unequivocally to the microlens which refracted it. In the classical SHWS, samples are required to lie in the photodetector area corresponding to a given microlens to remain localized, but the dynamic range of measurement becomes quite limited. To overcome this drawback, several authors have proposed different solutions for extending the dynamic range once the *f*-number is fixed [7-9].

2. WAVEFRONT SENSOR WITH EXTENDED DYNAMIC RANGE

To be able to measure highly aberrated wavefronts with abrupt shape changes we have developed a novel SHWS based on a cylindrical microlens array. The conventional array of spherical microlenses has been replaced with an array of microcylinders which focuses the wavefront to be measured onto the CCD in the form of focal lines instead of focal spots. This means that spots in a given focal line are now continuously connected, allowing us to perform a correct assignment of all the data, even in cases when the wavefront has locally important slope changes. This expansion of dynamic range using a cylindrical microlens array is illustrated in Fig. 1. Fig. 1a and Fig. 1b show, as an example, the spot distribution and vertical line pattern detected from a complex-shape wavefront passing through a conventional SHWS and through the sensor we present. As it may be seen, the part of the wavefront which is less aberrated and passes through the central column of the array of spherical microlenses (numbered as 1) or through the central microcylinder (1), is properly localized in both cases. However, to test the wavefront areas where steep shape changes are present, the cylindrical sensor enhances the performance of the conventional SHWS. Regarding areas labeled as 3 and 5, it may be seen how in the conventional SHWS the spots tagged with capital letters leave their original subapertures in area 3 and merge with those belonging to area 5. This implies an uncertainty in the assignment of spots a5 and A5, b5 and B?, and g5 and G5; and, consequently, these data gets lost for wavefront reconstruction. The use of an array of cylindrical microlenses solves this problem as all the wavefront samples refracted by each microcylinder are connected in the same focal line and may be easily tracked. Thus, samples within lines number 5 and number 3 are assigned to microcylinders 5 and 3, respectively.

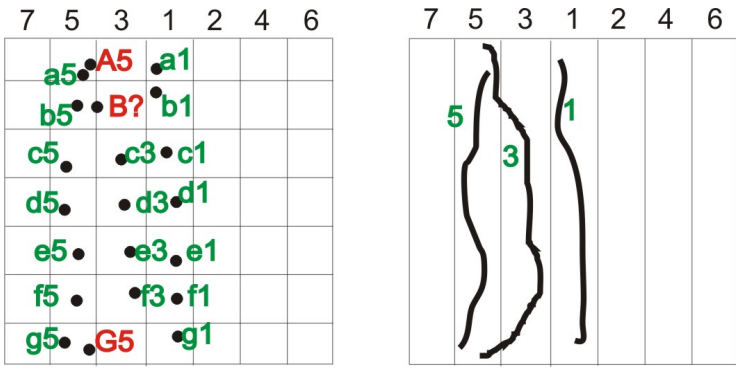

(a) (b)

Fig. 1. Example to illustrate the detected patterns of a complex wavefront with: (a) a conventional SHWS with spherical microlenses which has an uncertainty on the localization of spots a5 and A5, b5 and B?, and g5 and G5; and (b) our sensor based on an array of microcylinders from which all the data are correctly localized.

2.1. Setup

The wavefront sensor that we have developed is schematically depicted in Fig. 2. A 635 nm laser diode coupled with a monomode optical fiber acts as a point source which is collimated using a diffraction limited achromat. The collimated beam crosses the optical object of interest, and the transmitted wavefront is conjugated with a cylindrical microlens array through an afocal 4:1 beam reducer system. Microcylinders of f=10.9 mm focal length and d=500 µm width sample the wavefront creating a focal line pattern recorded by a ½" monochrome CCD detector of pixel dimensions p_x=p_y=4.65 µm. The array is placed onto a high-precision rotary stage, which allows the vertical and horizontal line patterns to be recorded.

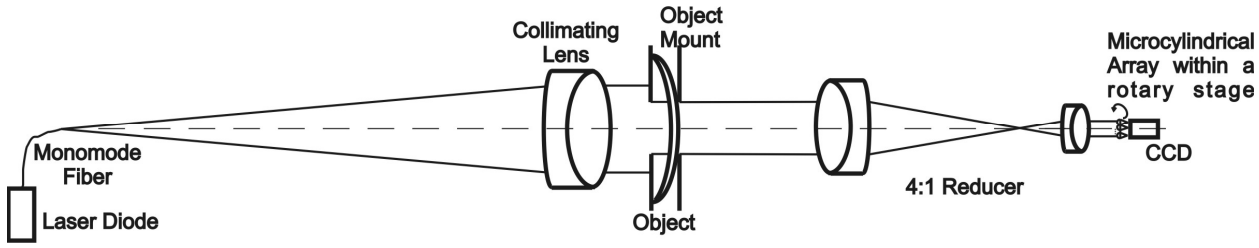

Fig. 2. Scheme of the setup constructed to test an ophthalmic lens by transmission with the cylindrical microlens array sensor.

2.2. Wavefront measurement procedure

Fig. 3 shows the complete measurement process from the line patterns detected to the reconstructed wavefront. Once the two orthogonal line patterns are captured, a processing algorithm is applied which localizes the lines even if they leave their corresponding microcylinder areas. First, in each line pattern a segmentation procedure separates the connected

active pixels from the background. Next, each of the resulting lines is tagged with ascending X and Y values starting from the central cylindrical microlens. Once each of the lines is tagged, both line patterns are superimposed and the areas with the active pixels of the intersection are obtained. These areas are equivalent to the spots of a conventional SHWS. The centroids ($\rho_x^{(X,Y)}$, $\rho_y^{(X,Y)}$) of these active areas are calculated using a classical center-of-mass computation, as follows:

$$\rho_x^{(X,Y)} = \frac{\sum_{(i,j)\in X\ fringe \cap Y\ fringe} I_{ij} \cdot i}{\sum_{(i,j)\in X\ fringe \cap Y\ fringe} I_{ij}}$$

$$\rho_y^{(X,Y)} = \frac{\sum_{(i,j)\in X\ fringe \cap Y\ fringe} I_{ij} \cdot j}{\sum_{(i,j)\in X\ fringe \cap Y\ fringe} I_{ij}} \qquad (1)$$

The wavefront slopes in the x and y directions (using the displacement of the aberrated centroids from the corresponding ones of the reference wavefront) are then calculated following the usual SHWS geometrical approximation

$$u^{(X,Y)} = \partial W / \partial x = M \cdot \frac{\left(\rho_{x,ABERR}^{(X,Y)} - \rho_{x,REF}^{(X,Y)}\right) \cdot p\_x}{f}$$

$$v^{(X,Y)} = \partial W / \partial y = M \cdot \frac{\left(\rho_{y,ABERR}^{(X,Y)} - \rho_{y,REF}^{(X,Y)}\right) \cdot p\_y}{f} \qquad (2)$$

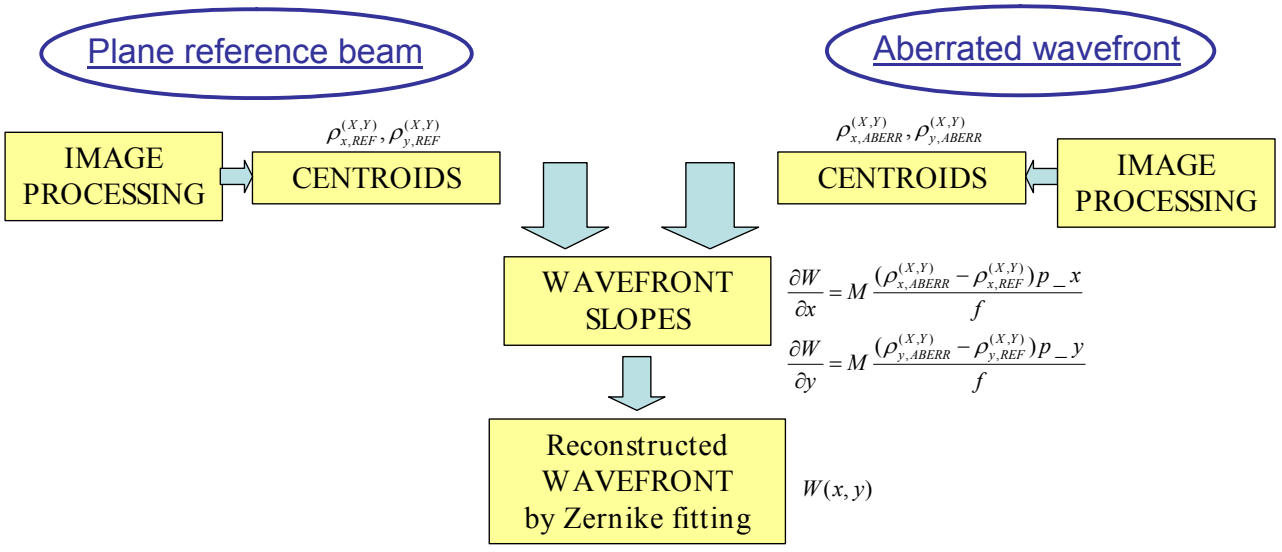

Fig. 3. Diagram of the wavefront measurement procedure with the described sensor

where M=1/4 is the magnification of the afocal system. From these data, the wavefront is finally reconstructed in terms of the circular Zernike polynomial decomposition [10,11].

3. EXPERIMENTAL RESULTS

3.1. Calibration of the sensor

The calibration of the sensor is a mandatory step to perform reliable absolute measurements. In a first approach, there are two main parameters in the sensor for which a difference in the real and nominal values may affect the accuracy of the measurement, namely the CCD pixel size and the spacing between the rear principal plane of the lenslet array and the CCD chip (which should equal the focal length of the microlenses) [12]. We chose to calibrate the sensor using the well-known spherical wavefront created by the fiber used as the point light source of our system. The fiber tip was placed 535 mm in front of the object plane of the 4:1 beam reducer. By simply removing the collimating lens, the divergent spherical wavefront with a well-known 535 mm radius of curvature (ROC) must be sensed. The reference beam for the sensor was obtained through the plane wave created when the achromat is working as a collimator, without any test object present. This calibration procedure has two main advantages: a) the same collimated wavefront used as the reference in the calibration will be used when measuring any phase object, and b) a high quality spherical wavefront has been used for calibration without any mechanical changes to the setup, so avoiding the introduction of potential errors in position and alignment.

Experimental results for the calibration procedure are presented in Fig. 4, where the displacement of the reference and the aberrated centroids for the x and y pupil positions may be appreciated. By means of a linear fit of the displacement of the reference and the aberrated centroids for the x *(y)* positions, the curvature, C, of the measured spherical wavefront multiplied by the $\left(p - x/f\right)^{-1}$ ($\left(p - y/f\right)^{-1}$) factor was obtained, yielding $C \cdot \left(p - x/f\right)^{-1} = 63.83\ \text{mm}^{-1}$ and $C \cdot \left(p - y/f\right)^{-1} = 63.80\ \text{mm}^{-1}$, respectively. Considering that the reference curvature of the spherical wavefront is $C = \left(ROC \cdot M^2\right)^{-1} = \left(535 \cdot 1/4^2\right)^{-1}$ mm^{-1} because of the 4:1 afocal reducer, we got $p - x/f$ and $p - y/f$ calibrated values of 4.685 x 10^{-4} and 4.687 x 10^{-4}.

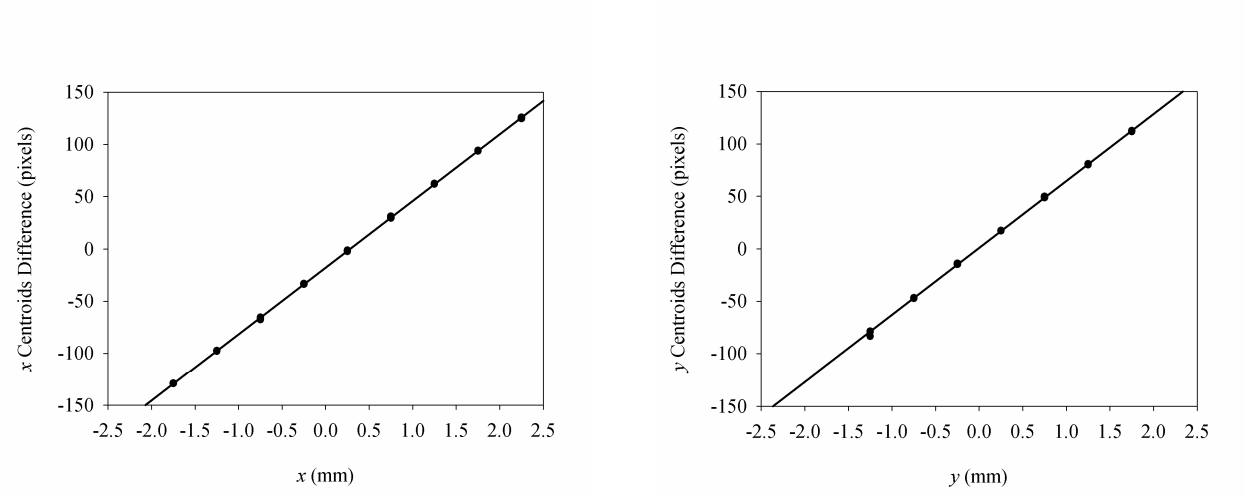

Fig. 4. Calibration of the sensor by means of the measurement of a well-known spherical wavefront: linear fit of the displacement between the aberrated and reference centroids versus the x (left plot) and y (right plot) positions.

The spherical wavefront measurement was also used to compute the sensitivity (or vertical resolution) of the sensor, defined as the smallest amount of wavefront aberration that the sensor can reliably measure. Ten successive measurements were taken. From these, the root mean square (RMS) difference between the measured u and v slopes and the average slopes was calculated. A RMS value of 0.017 mrad was obtained. From that slope sensitivity, calculating the sensitivity of the sensor in terms of the wavefront is straightforward using the relation proposed by Neal *et al.* [13]:

$$RMS\ wavefront\ error = (RMS\ slope\ error)d\sqrt{N} \tag{3}$$

where N is the number of samples, and d the width of the microlenses. This results in a sensitivity of $\lambda/25$ at the wavelength used (λ=635 nm).

3.2. Single shot measurement of an ophthalmic progressive addition lens

To show the capabilities of the sensor, we measured a commercial progressive addition lens (PAL) which had a nominal null far vision power and +2D power addition. In a single shot, a 20 mm diameter area was inspected, covering the power progression corridor and part of the lateral blurred zones where considerable astigmatism is present. The intersection between the two orthogonal line patterns recorded by the CCD is shown in Fig. 5.a. The deflection of the focal lines visually shows the power progression of the PAL from the neutral distance vision area to the highest-power near vision area. As expected, in the regions where the wavefront is more aberrated, the width of the focal line increases from the diffraction-limited size and is also displaced outside the corresponding microcylinder area on the CCD array.

From the 74 *u* and *v* pairs measured, we performed the wavefront reconstruction in terms of the circular Zernike polynomial basis. Fig. 5.b clearly shows how the wavefront is almost flat in the far vision area and increases its curvature along the corridor following the increase in lens power. The distribution of astigmatic aberrations in the lateral areas of the vertical corridor is also correctly reproduced. Notice that the measured peak-to-valley value of more than 80λ reveals the huge dynamic range of the sensor.

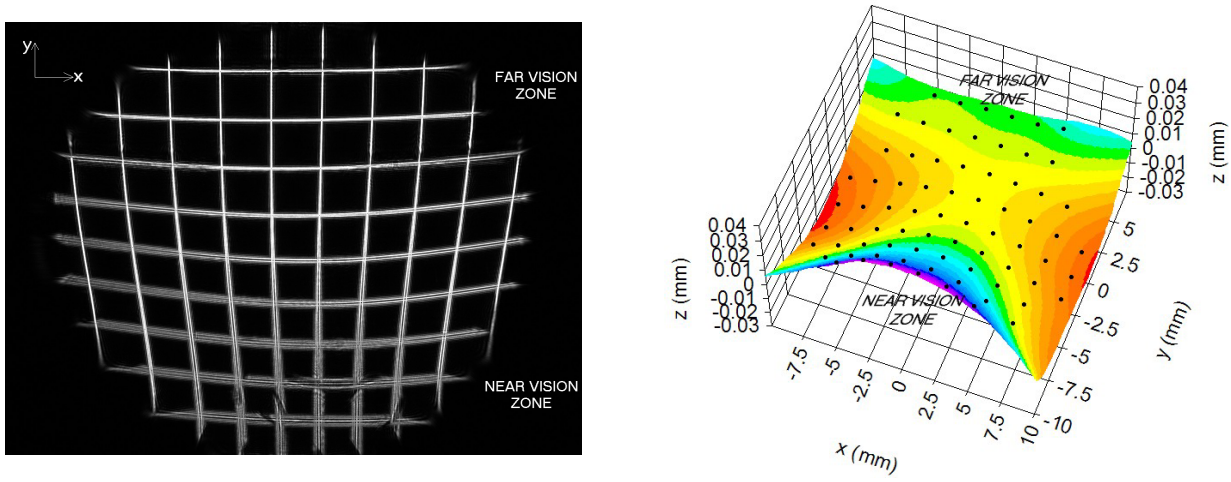

(a) (b)

Fig. 5. Commercial progressive addition lens (PAL) measured with the sensor: (a) intersection of the detected line patterns in *x* and *y* directions, (b) reconstruction of the wavefront transmitted by the PAL.

4. CONCLUSIONS AND FUTURE WORK

We have developed a novel Shack-Hartmann type wavefront sensor based on a cylindrical microlens array for testing new commercial optics with complex shapes. The use of cylindrical microlenses combined with the image processing algorithm presented extends the dynamic range of the conventional SHWS sensor without degrading the resolution ($\lambda/25$ at λ=635 nm), allowing the measurement of highly aberrated wavefronts with steep shape variations. As an example, a wavefront transmitted by a commercial PAL with more than 80λ peak-to-valley height was tested with the sensor to demonstrate its performance in the measurement of complex-shape wavefronts.

Two important improvements in the system presented are now being implemented out in order to increase the spatial resolution and the measurement speed of the setup. A new cylindrical array with microlenses of 300 μm width is now

being introduced, which will allow to almost duplicate the current spatial resolution. On the other hand, the single microcylindrical array mounted in a high-precision rotary stage is being substituted by two equal microcylindrical arrays placed vertically and horizontally, respectively, allowing the simultaneous detection of both orthogonal line patterns, in order to yield a real single-shot measurement.

ACKNOWLEDMENTS

The authors would like to thank the Spanish Ministry of Education and Science for the AP2003-3140 grant received, and for the project DPI2005-00828, which has partially funded this research.

REFERENCES

1. G. Young Yoon, T. Jitsuno, M. Nakatsuka and S. Nakai, "Shack Hartmann wave-front measurement with a large F-number plastic microlens array", Appl. Opt., 35 (1), pp.188-192, 1996.

2. T.M. Jeong, M. Menon and G. Yoon, "Measurement of wave-front aberration in soft contact lenses by use of a Shack-Hartmann wave-front sensor", Appl. Opt., 44 (21), pp.4523-4527, 2005.

3. M. Beyerlein, J. Pfund, "Shack-Hartmann wavefront sensors move into new applications", Laser Focus World, 42 (4), pp.90-93, 2006.

4. J. Primot, G. Rousset and J.C. Fontanella, "Deconvolution from wave-front sensing - a new technique for compensating turbulence-degraded images", J. Opt. Soc. Am. A, 7 (9), pp.1598-1608, 1990.

5. L. Seifert, H.J. Tiziani and W. Osten, "Wavefront reconstruction with the adaptive Shack-Hartmann sensor", Opt. Comm., 245, pp.255-269, 2005.

6. R.R. Rammage, D.R. Neal and R.J. Copland, "Application of Shack-Hartmann wavefront sensing technology to transmissive optic metrology", Advanced Characterization Techniques for Optical, Semiconductor, and Data Storage Components, Proc. SPIE 4779, pp.161-172, 2002.

7. S. Groening, B. Sick, K. Donner, J. Pfund, N. Lindlein and J. Schwider, "Wave-front reconstruction with a Shack-Hartmann sensor with an iterative spline fitting method", Appl. Opt., 39 (4), pp.561-567, 2000.

8. N. Lindlein and J. Pfund, "Experimental results for expanding the dynamic range of a Shack-Hartmann sensor using astigmatic microlenses ", Opt. Eng., 41 (2), pp.529-533, 2002.

9. J. Lee, R.V. Shack and M.R. Descour, "Sorting method to extend the dynamic range of the Shack-Hartmann wave-front sensor", Appl. Opt., 44 (23), pp.4838-4845, 2005.

10. D. Malacara and S. L. DeVore, "Optical Shop Testing" 2nd Ed., Wiley, New York, 1992.

11. M.Ares and S.Royo, "Comparison of cubic B-Spline and Zernike fitting techniques in complex wavefront reconstruction", Appl.Opt., 45 (27), pp.6954-6964, 2006.

12. A. Chernyshov, U. Sterr, F. Riehle, J. Helmcke and J. Pfund, "Calibration of a Shack-Hartmann sensor for absolute measurements of wavefronts", Appl. Opt., 44 (30), pp.6419-6425, 2005.

13. D.R. Neal, D.J. Armstrong and W.T. Turner, "Wavefront sensors for control and process monitoring in optics manufacture", Proc. SPIE 2993, pp.211-220, 1997.